3-D ADI–FDTD Method—Unconditionally Stable Time-Domain Algorithm for Solving Full Vector Maxwell's Equations

Takefumi Namiki, *Member, IEEE*

***Abstract*—We previously introduced the alternating direction implicit finite-difference time-domain (ADI–FDTD) method for a two-dimensional TE wave. We analytically and numerically verified that the algorithm of the method is unconditionally stable and free from the Courant–Friedrich–Levy condition restraint. In this paper, we extend this approach to a full three-dimensional (3-D) wave. Numerical formulations of the 3-D ADI–FDTD method are presented and simulation results are compared to those using the conventional 3-D finite-difference time-domian (FDTD) method. We numerically verify that the 3-D ADI–FDTD method is also unconditionally stable and it is more efficient than the conventional 3-D FDTD method in terms of the central processing unit time if the size of the local minimum cell in the computational domain is much smaller than the other cells and the wavelength.**

***Index Terms*—ADI–FDTD method, CFL condition, FDTD method.**

I. Introduction

THE finite-difference time-domain (FDTD) method [1], [2] is widely used for solving problems related to electromagnetism. As the traditional FDTD method is based on an explicit finite-difference algorithm, the Courant–Friedrich–Levy (CFL) condition [2] must be satisfied when this method is used. Therefore, a maximum time-step size is limited by minimum cell size in a computational domain, which means that if an object of analysis has fine scale dimensions compared with wavelength, a small time-step size creates a significant increase in calculation time.

We previously introduced the alternating direction implicit finite-difference time-domain (ADI–FDTD) method for solving the two-dimensional TE wave [3]. The method is based on the alternating direction implicit (ADI) method [4] and is applied to Yee's staggered cell [1] to solve Maxwell's equations. We analytically demonstrated that the growth factor of the algorithm is always unity, i.e., this scheme is unconditionally stable and is not dissipative. Therefore, the time-step size can be arbitrarily set when this method is used. The limitation of the maximum time-step size of the method does not depend on the CFL condition, but rather on numerical errors.

We extended this approach to a full three-dimensional (3-D) wave and introduced the 3-D ADI–FDTD method [5]. In this paper, we explain the details of numerical formulations of the ADI FDTD method for a 3-D full vector wave and demonstrate some numerical examples.

Manuscript received October 5, 1999.

The author is with the Computational Science and Engineering Center, Fujitsu Ltd., Chiba 261-8588, Japan (e-mail: namiki@strad.se.fujitsu.co.jp).

Publisher Item Identifier S 0018-9480(00)08727-5.

II. Numerical Formulations of the 3-D ADI–FDTD Method

The numerical formulation of the ADI–FDTD method for a full 3-D wave is presented in (1)–(12). The electromagnetic-field components are arranged on the cells in the same way as that using the conventional FDTD method. These formulations are available for inhomogeneous lossy medium and for using nonuniform cells. The calculation for one discrete time step is performed using two procedures. The first procedure is based on (1)–(6) and the second procedure is based on (7)–(12) as follows:

⟨First procedure⟩

$$\begin{aligned} Ex^{n+1/2}_{(i+1/2,j,k)} &= Ca_{(i+1/2,j,k)} \cdot Ex^{n}_{(i+1/2,j,k)} + Cb_{(i+1/2,j,k)} \\ &\quad \cdot \left[\left\{ Hz^{n}_{(i+1/2,j+1/2,k)} - Hz^{n}_{(i+1/2,j-1/2,k)} \right\} \Big/ \Delta y(j) \right. \\ &\quad \left. - \left\{ Hy^{n+1/2}_{(i+1/2,j,k+1/2)} - Hy^{n+1/2}_{(i+1/2,j,k-1/2)} \right\} \Big/ \Delta z(k) \right] \end{aligned} \tag{1}$$

$$\begin{aligned} Ey^{n+1/2}_{(i,j+1/2,k)} &= Ca_{(i,j+1/2,k)} \cdot Ey^{n}_{(i,j+1/2,k)} + Cb_{(i,j+1/2,k)} \\ &\quad \cdot \left[\left\{ Hx^{n}_{(i,j+1/2,k+1/2)} - Hx^{n}_{(i,j+1/2,k-1/2)} \right\} \Big/ \Delta z(k) \right. \\ &\quad \left. - \left\{ Hz^{n+1/2}_{(i+1/2,j+1/2,k)} - Hz^{n+1/2}_{(i-1/2,j+1/2,k)} \right\} \Big/ \Delta x(i) \right] \end{aligned} \tag{2}$$

$$\begin{aligned} Ez^{n+1/2}_{(i,j,k+1/2)} &= Ca_{(i,j,k+1/2)} \cdot Ez^{n}_{(i,j,k+1/2)} + Cb_{(i,j,k+1/2)} \\ &\quad \cdot \left[\left\{ Hy^{n}_{(i+1/2,j,k+1/2)} - Hy^{n}_{(i-1/2,j,k+1/2)} \right\} \Big/ \Delta x(i) \right. \\ &\quad \left. - \left\{ Hx^{n+1/2}_{(i,j+1/2,k+1/2)} - Hx^{n+1/2}_{(i,j-1/2,k+1/2)} \right\} \Big/ \Delta y(j) \right] \end{aligned} \tag{3}$$

$$\begin{aligned} Hx^{n+1/2}_{(i,j+1/2,k+1/2)} &= Hx^{n}_{(i,j+1/2,k+1/2)} + Db_{(i,j+1/2,k+1/2)} \\ &\quad \cdot \left[\left\{ Ey^{n}_{(i,j+1/2,k+1)} - Ey^{n}_{(i,j+1/2,k)} \right\} \Big/ \Delta z(k) \right. \\ &\quad \left. - \left\{ Ez^{n+1/2}_{(i,j+1,k+1/2)} - Ez^{n+1/2}_{(i,j,k+1/2)} \right\} \Big/ \Delta y(j) \right] \end{aligned} \tag{4}$$

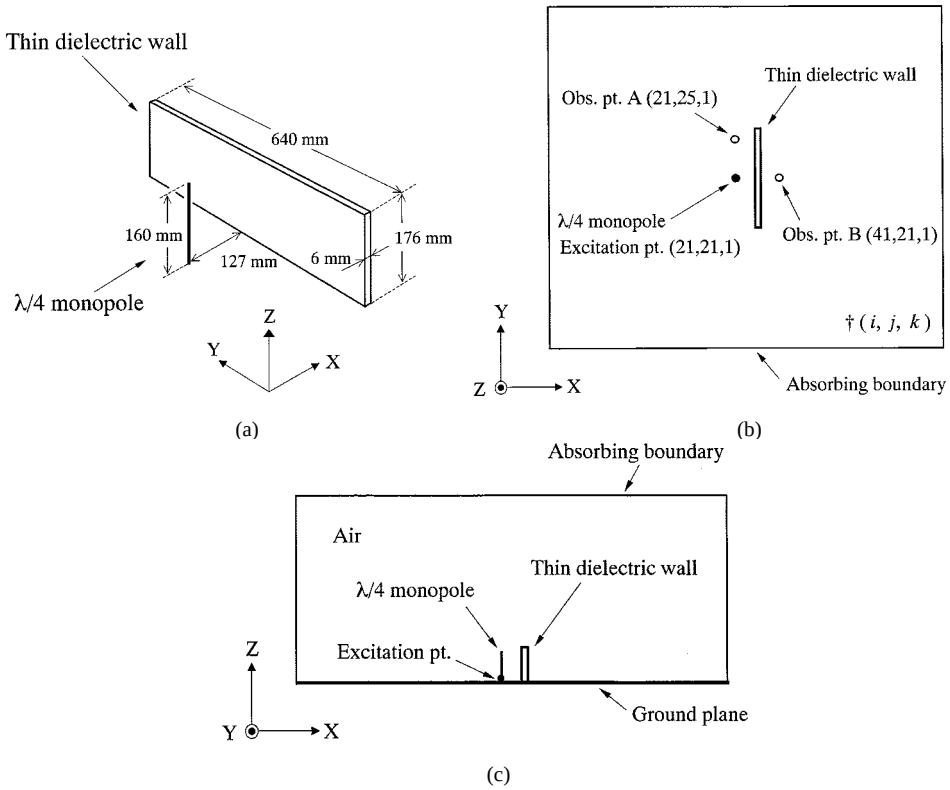

Fig. 1. Monopole antenna near a thin dielectric wall. (a) Bird's eye view. (b) Horizontal view. (c) Vertical view.

$$Hy^{n+1/2}_{(i+1/2,j,k+1/2)} = Hy^{n}_{(i+1/2,j,k+1/2)} + Db_{(i+1/2,j,k+1/2)} \cdot \left[\left\{ Ez^{n}_{(i+1,j,k+1/2)} - Ez^{n}_{(i,j,k+1/2)} \right\} \Big/ \Delta x(i) - \left\{ Ex^{n+1/2}_{(i+1/2,j,k+1)} - Ex^{n+1/2}_{(i+1/2,j,k)} \right\} \Big/ \Delta z(k) \right] \quad (5)$$

$$Hz^{n+1/2}_{(i+1/2,j+1/2,k)} = Hz^{n}_{(i+1/2,j+1/2,k)} + Db_{(i+1/2,j+1/2,k)} \cdot \left[\left\{ Ex^{n}_{(i+1/2,j+1,k)} - Ex^{n}_{(i+1/2,j,k)} \right\} \Big/ \Delta y(j) - \left\{ Ey^{n+1/2}_{(i+1,j+1/2,k)} - Ey^{n+1/2}_{(i,j+1/2,k)} \right\} \Big/ \Delta x(i) \right] \quad (6)$$

⟨Second procedure⟩

$$Ex^{n+1}_{(i+1/2,j,k)} = Ca_{(i+1/2,j,k)} \cdot Ex^{n+1/2}_{(i+1/2,j,k)} + Cb_{(i+1/2,j,k)} \cdot \left[\left\{ Hz^{n+1}_{(i+1/2,j+1/2,k)} - Hz^{n+1}_{(i+1/2,j-1/2,k)} \right\} \Big/ \Delta y(j) - \left\{ Hy^{n+1/2}_{(i+1/2,j,k+1/2)} - Hy^{n+1/2}_{(i+1/2,j,k-1/2)} \right\} \Big/ \Delta z(k) \right] \quad (7)$$

$$Ey^{n+1}_{(i,j+1/2,k)} = Ca_{(i,j+1/2,k)} \cdot Ey^{n+1/2}_{(i,j+1/2,k)} + Cb_{(i,j+1/2,k)} \cdot \left[\left\{ Hx^{n+1}_{(i,j+1/2,k+1/2)} - Hx^{n+1}_{(i,j+1/2,k-1/2)} \right\} \Big/ \Delta z(k) - \left\{ Hz^{n+1/2}_{(i+1/2,j+1/2,k)} - Hz^{n+1/2}_{(i-1/2,j+1/2,k)} \right\} \Big/ \Delta x(i) \right] \quad (8)$$

$$Ez^{n+1}_{(i,j,k+1/2)} = Ca_{(i,j,k+1/2)} \cdot Ez^{n+1/2}_{(i,j,k+1/2)} + Cb_{(i,j,k+1/2)} \cdot \left[\left\{ Hy^{n+1}_{(i+1/2,j,k+1/2)} - Hy^{n+1}_{(i-1/2,j,k+1/2)} \right\} \Big/ \Delta x(i) - \left\{ Hx^{n+1/2}_{(i,j+1/2,k+1/2)} - Hx^{n+1/2}_{(i,j-1/2,k+1/2)} \right\} \Big/ \Delta y(j) \right] \quad (9)$$

$$Hx^{n+1}_{(i,j+1/2,k+1/2)} = Hx^{n+1/2}_{(i,j+1/2,k+1/2)} + Db_{(i,j+1/2,k+1/2)} \cdot \left[\left\{ Ey^{n+1}_{(i,j+1/2,k+1)} - Ey^{n+1}_{(i,j+1/2,k)} \right\} \Big/ \Delta z(k) - \left\{ Ez^{n+1/2}_{(i,j+1,k+1/2)} - Ez^{n+1/2}_{(i,j,k+1/2)} \right\} \Big/ \Delta y(j) \right] \quad (10)$$

$$Hy^{n+1}_{(i+1/2,j,k+1/2)} = Hy^{n+1/2}_{(i+1/2,j,k+1/2)} + Db_{(i+1/2,j,k+1/2)} \cdot \left[\left\{ Ez^{n+1}_{(i+1,j,k+1/2)} - Ez^{n+1}_{(i,j,k+1/2)} \right\} \Big/ \Delta x(i) - \left\{ Ex^{n+1/2}_{(i+1/2,j,k+1)} - Ex^{n+1/2}_{(i+1/2,j,k)} \right\} \Big/ \Delta z(k) \right] \quad (11)$$

$$Hz^{n+1}_{(i+1/2,j+1/2,k)} = Hz^{n+1/2}_{(i+1/2,j+1/2,k)} + Db_{(i+1/2,j+1/2,k)} \cdot \left[\left\{ Ex^{n+1}_{(i+1/2,j+1,k)} - Ex^{n+1}_{(i+1/2,j,k)} \right\} \Big/ \Delta y(j) - \left\{ Ey^{n+1/2}_{(i+1,j+1/2,k)} - Ey^{n+1/2}_{(i,j+1/2,k)} \right\} \Big/ \Delta x(i) \right]. \quad (12)$$

The coefficients are defined in the same way as in the conventional FDTD method and they are as follows:

$$C_a(i,j,k) = \frac{2\varepsilon(i,j,k) - \sigma(i,j,k)\,\Delta t}{2\varepsilon(i,j,k) + \sigma(i,j,k)\,\Delta t}$$
$$C_b(i,j,k) = \frac{2\Delta t}{2\varepsilon(i,j,k) + \sigma(i,j,k)\,\Delta t}$$
$$D_b(i,j,k) = \frac{\Delta t}{\mu(i,j,k)}.$$

None of these equations can be used for direct numerical calculation because they include the components defined as synchronous variables on both the left- and right-hand side, thus, modified equations are derived from the original equations.

In the first procedure, the E_x component on the left-hand side and the H_y components on the right-hand side are defined as synchronous variables in (1), thus, a modified (1′) for the E_x component is derived from (1) and (5) by eliminating the $H_y^{n+1/2}$ components. In the suffix k, (1′) indicates k maximum number of simultaneous linear equations and also means z-directional scan of the E_x components as follows:

$$\begin{aligned}
&-\alpha_1 Ex^{n+1/2}_{(i+1/2,j,k-1)} + \beta_1 Ex^{n+1/2}_{(i+1/2,j,k)} - \gamma_1 Ex^{n+1/2}_{(i+1/2,j,k+1)} \\
&\quad = p_1 Ex^{n}_{(i+1/2,j,k)} \\
&\qquad + \left\{ Hz^{n}_{(i+1/2,j+1/2,k)} - Hz^{n}_{(i+1/2,j-1/2,k)} \right\} \Big/ \Delta y(j) \\
&\qquad\quad - \left\{ Hy^{n}_{(i+1/2,j,k+1/2)} - Hy^{n}_{(i+1/2,j,k-1/2)} \right\} \Big/ \Delta z(k) \\
&\qquad + q_1 \left\{ Ez^{n}_{(i+1,j,k-1/2)} - Ez^{n}_{(i,j,k-1/2)} \right\} \Big/ \{\Delta x(i)\Delta z(k)\} \\
&\qquad - r_1 \left\{ Ez^{n}_{(i+1,j,k+1/2)} - Ez^{n}_{(i,j,k+1/2)} \right\} \Big/ \{\Delta x(i)\Delta z(k)\}
\end{aligned} \tag{1′}$$

where

$$\begin{aligned}
\alpha_1 &= Db_{(i+1/2,j,k-1/2)}/\Delta z(k)^2 \\
\beta_1 &= 1/Cb_{(i+1/2,j,k)} + \alpha_1 + \gamma_1 \\
\gamma_1 &= Db_{(i+1/2,j,k+1/2)}/\Delta z(k)^2 \\
p_1 &= Ca_{(i+1/2,j,k)}/Cb_{(i+1/2,j,k)} \\
q_1 &= Db_{(i+1/2,j,k-1/2)} \\
r_1 &= Db_{(i+1/2,j,k+1/2)}.
\end{aligned}$$

In the same way, the modified equation for the $E_y^{n+1/2}$ component, which indicates i maximum number of simultaneous linear equations and also means x-directional scan of the E_y components, is derived from (2) and (6). Also, the modified equation for the $E_z^{n+1/2}$ component, which indicates j maximum number of simultaneous linear equations and also means y-directional scan of the E_z components, is derived from (3) and (4). By solving their simultaneous linear equations, we can get the values of the electric-field components at the time of $n+1/2$. Thereafter, we can get the values of the magnetic-field components at the time of $n+1/2$ directly from (4)–(6).

In the second procedure, the E_x component on the left-hand side and the H_z components on the right-hand side are defined as synchronous variables in (7), thus, a modified (7′) for the E_x component is derived from (7) and (12) by eliminating the H_z^{n+1} components. In the suffix j, (7′) indicates j maximum number of simultaneous linear equations and also means y-directional scan of the E_x components.

$$\begin{aligned}
&-\alpha_2 Ex^{n+1}_{(i+1/2,j-1,k)} + \beta_2 Ex^{n+1}_{(i+1/2,j,k)} - \gamma_2 Ex^{n+1}_{(i+1/2,j+1,k)} \\
&\quad = p_2 Ex^{n+1/2}_{(i+1/2,j,k)} \\
&\qquad + \left\{ Hz^{n+1/2}_{(i+1/2,j+1/2,k)} - Hz^{n+1/2}_{(i+1/2,j-1/2,k)} \right\} \Big/ \Delta y(j) \\
&\qquad\quad - \left\{ Hy^{n+1/2}_{(i+1/2,j,k+1/2)} - Hy^{n+1/2}_{(i+1/2,j,k-1/2)} \right\} \Big/ \Delta z(k) \\
&\qquad + q_2 \left\{ Ey^{n+1/2}_{(i+1,j-1/2,k)} - Ey^{n+1/2}_{(i,j-1/2,k)} \right\} \Big/ \{\Delta x(i)\Delta y(j)\} \\
&\qquad - r_2 \left\{ Ey^{n+1/2}_{(i+1,j+1/2,k)} - Ey^{n+1/2}_{(i,j+1/2,k)} \right\} \Big/ \{\Delta x(i)\Delta y(j)\}
\end{aligned} \tag{7′}$$

where

$$\begin{aligned}
\alpha_2 &= Db_{(i+1/2,j-1/2,k)}/\Delta y(j)^2 \\
\beta_2 &= 1/Cb_{(i+1/2,j,k)} + \alpha_2 + \gamma_2 \\
\gamma_2 &= Db_{(i+1/2,j+1/2,k)}/\Delta y(j)^2 \\
p_2 &= Ca_{(i+1/2,j,k)}/Cb_{(i+1/2,j,k)} \\
q_2 &= Db_{(i+1/2,j-1/2,k)} \\
r_2 &= Db_{(i+1/2,j+1/2,k)}.
\end{aligned}$$

In the same way, the modified equation for the E_y^{n+1} component, which indicates k maximum number of simultaneous linear equations and also means z-directional scan of the E_y components, is derived from (8) and (10). Also, the modified equation for the E_z^{n+1} component, which indicates i maximum number of simultaneous linear equations and also means x-directional scan of the E_z components, is derived from (9) and (11). By solving their simultaneous linear equations, we can get the values of the electric-field components at the time of $n+1$. Thereafter, we can get the values of the magnetic-field components at the time of $n+1$ directly from (10)–(12).

Since the simultaneous linear equations such as (1′) and (7′) can be written in a tridiagonal matrix form, and their coefficients on the left-hand side satisfy $|\beta| > |\alpha| + |\gamma|$, the computational costs to solve the equations are not very significant [6].

We note that there is no necessity to scan the E_x, E_y, and E_z components in the x-, y-, and z-directions, respectively, because an electromagnetic wave is a transverse wave.

III. Numerical Example

In order to demonstrate the above 3-D ADI–FDTD method, two examples are presented. Numerical simulations were carried out using both the 3-D ADI–FDTD method and the conventional 3-D FDTD method for comparison.

A. Monopole Antenna Near a Thin Dielectric Wall

Fig. 1 shows numerical model of a $\lambda/4$ monopole antenna mounted near a thin dielectric wall. The 160-mm-long monopole antenna was mounted near the 1-mm-thick 640-mm-wide 176-mm-high dielectric wall on an infinite ground plane. The distance between the antenna and the wall surface was 127 mm. Observation points A and B were at a 25.6 and 26.0 mm distance from the antenna, respectively. Mur's first-order absorbing boundary condition [7] was set

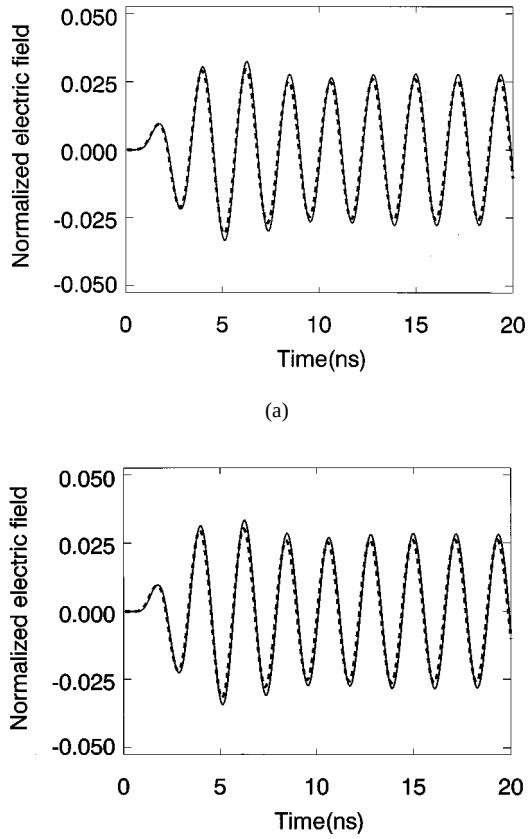

Fig. 2 Normalized electric field when the electric characteristics of the wall were set as $\varepsilon_r = 4.0$, $\mu_r = 1.0$, and $\sigma = 0.0$ S/m. (a) At point A. (b) At point B. (Solid line: conventional FDTD. Dashed line: ADI–FDTD.)

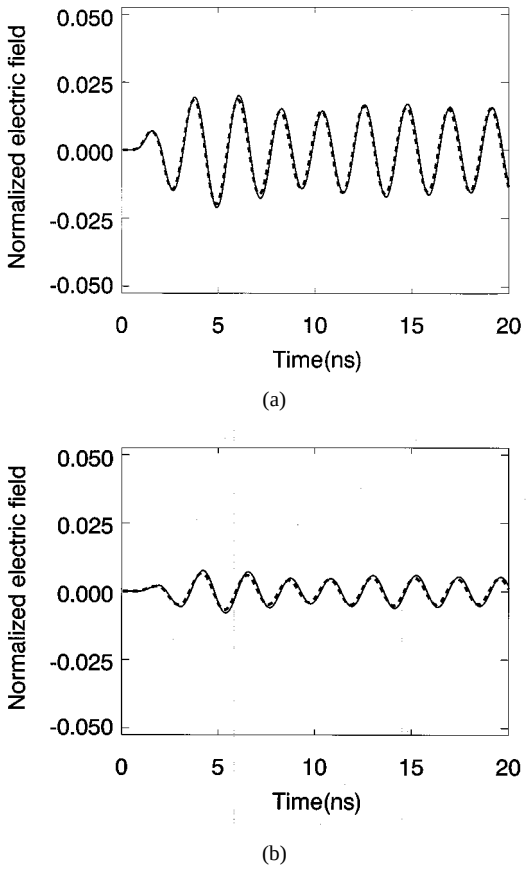

Fig. 3 Normalized electric field when the electric characteristics of the wall were set as $\varepsilon_r = 4.0$, $\mu_r = 1.0$, and $\sigma = 4.0$ S/m. (a) At point A. (b) At point B. (Solid line: conventional FDTD. Dashed line: ADI–FDTD.)

on the outer surfaces, except the bottom ground plane. The perfect-electric-conductor boundary condition was set at the antenna and ground plane.

We used nonuniform cells so as to treat the thin dielectric wall and relatively wide computational domain. The detail of the cell size was as follows:

$$dx(i) = \begin{cases} 64\text{ mm} & (1 \le i \le 21) \quad dx(i) : \text{constant} \\ 2 - 32\text{ mm} & (22 \le i \le 26) \quad dx(i+1) = dx(i)/2 \\ 1\text{ mm} & (27 \le i \le 34) \quad dx(i) : \text{constant} \\ 32 - 2\text{ mm} & (35 \le i \le 39) \quad dx(i+1)/2 = dx(i) \\ 64\text{ mm} & (40 \le i \le 58) \quad dx(i) : \text{constant} \end{cases}$$

$$dy(j) = 64\text{ mm} \quad (1 \le j \le 40) \quad dy(j) : \text{constant}$$

$$dz(k) = \begin{cases} 8\text{ mm} & (1 \le k \le 22) \quad dz(k) : \text{constant} \\ 16\text{ mm} & (k = 23) \quad dz(k) : \text{constant} \\ 32\text{ mm} & (k = 24) \quad dz(k) : \text{constant} \\ 64\text{ mm} & (25 \le k \le 42) \quad dz(k) : \text{constant}. \end{cases}$$

The size of cells at the air region was set at 64 mm, which was about $\lambda/10$. The minimum size of cells, which was set at around the wall, was $1 \times 8 \times 64$ mm^3 in this model, thus, the CFL condition was $\Delta t \le 3.3071954$ ps. The time-step size was set as 3.307 ps for the conventional FDTD and 66.140 ps for the ADI–FDTD.

First, a continuous sinusoidal wave, the frequency and wavelength of which were 460 MHz and 652 mm, respectively, was excited at the E_z component of the bottom cell of the antenna. The E_z components at observation points A and B were output. We calculated twice for different electric characteristics of the dielectric wall. The output E_z components at points A and B normalized by the value of the excited amplitude, when the electric characteristics of the wall were set as $\varepsilon_r = 4.0$, $\mu_r = 1.0$, and $\sigma = 0.0$ S/m are shown in Fig. 2(a) and (b), respectively. The output E_z components, when the electric characteristics of the wall were set as $\varepsilon_r = 4.0$, $\mu_r = 1.0$, $\sigma = 4.0$ S/m, are shown in Fig. 3(a) and (b), respectively. The results in the ADI–FDTD case and conventional FDTD case were in good agreement.

Next, a Gaussian pulse was excited at the E_z component of the bottom cell of the antenna, and the E_z component at observation point B was output. Numerical simulations were performed twice, with and without the wall that had the electric characteristics of $\varepsilon_r = 4.0$, $\mu_r = 1.0$, and $\sigma = 4.0$ S/m. By applying a Fourier transformation to each output field, the shielding effectiveness values were calculated. The normalized E_z components versus time are shown in Fig. 4 and the shielding effectiveness values versus frequency are shown in Fig. 5. The results in the ADI–FDTD case and conventional FDTD case were also in good agreement.

These simulations were performed on an Ultra SPARC II 360-MHz workstation. The CPU time and required memory size of these simulations are shown in Table I, with the time-step size and total time steps. In the case of the ADI–FDTD, the time-step size can be set 20 times as large as the conventional FDTD, and total time steps can be reduced by a factor of 20. The CPU time

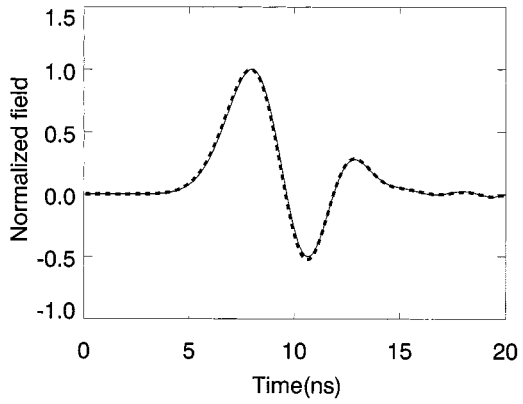

Fig. 4. Normalized electric field at point B when a Gaussian pulse was excited. (Solid line: conventional FDTD. Dashed line: ADI–FDTD.)

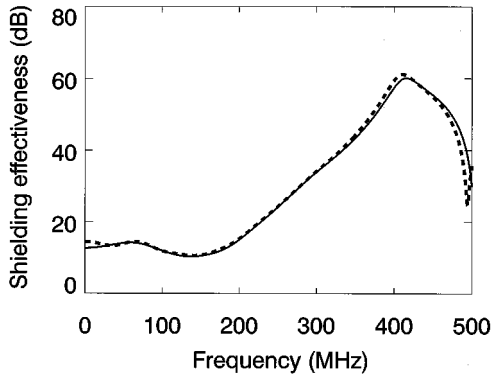

Fig. 5. Shielding effectiveness versus frequency. (Solid line: conventional FDTD. Dashed line: ADI–FDTD.)

TABLE I
INFORMATION ON THE MONOPOLE ANTENNA SIMULATION

	Δt	Steps	CPU Time	Memory
FDTD	3.307 ps	6600	221.4 s	6.8 Mb
ADI-FDTD	66.14 ps	330	53.2 s	13.1 Mb

is also reduced to 24%. Required memory size, which is about 1.9 times, is increased because of the necessity for extra array storage.

B. Stripline with a Narrow Gap

Fig. 6 shows numerical models of a stripline with a narrow gap. The ground planes were separated by 2.4 mm. The strip in the center of them was 1.2-mm wide and the electric characteristics of the medium between them were $\varepsilon_r = 4.0$, $\mu_r = 1.0$, and $\sigma = 0.0$ S/m. The 25-μm gap was in the center of the strip and four cells were applied there. Mur's first-order absorbing boundary condition was set at z-directional terminals. The perfect-electric-conductor boundary condition was set at the strip

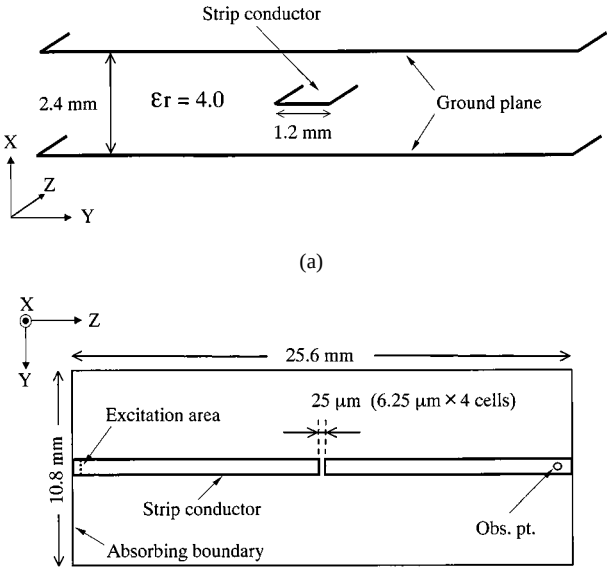

Fig. 6 Stripline structure (a) Vertical view. (b) Horizontal view.

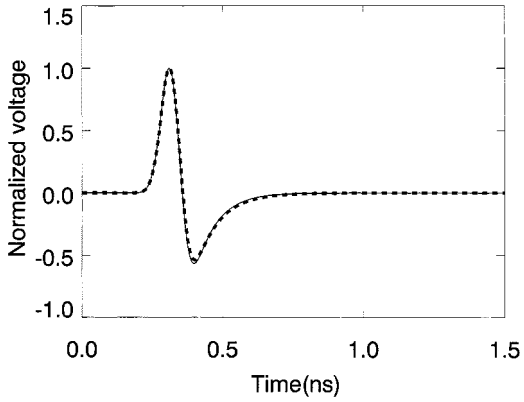

Fig. 7. Normalized output voltage at observation point. (Solid line: conventional FDTD. Dashed line: ADI–FDTD ($\Delta t = 1.0410$ ps).)

and ground planes. A Gaussian pulse was excited at the excitation area and the E_x components at the observation point were output.

We used nonuniform cells so as to treat the narrow gap and long strip line. The detail of the cell size was as follows:

$$dx(i) = 0.4\ \text{mm} \quad (1 \le i \le 6) \quad dx(i)\ \text{: constant}$$

$$dy(j) = 0.2\ \text{mm} \quad (1 \le j \le 54) \quad dy(j)\ \text{: constant}$$

$$dz(k) = \begin{cases} 0.4\ \text{mm} & (1 \le k \le 31) \quad dz(k)\ \text{: constant} \\ 0.2-0.0125\ \text{mm} & (32 \le k \le 36) \quad dz(k+1) = dz(k)/2 \\ 0.00625\ \text{mm} & (37 \le k \le 40) \quad dz(k)\ \text{: constant} \\ 0.0125-0.2\ \text{mm} & (41 \le k \le 45) \quad dz(k+1)/2 = dz(k) \\ 0.4\ \text{mm} & (46 \le k \le 76) \quad dz(k)\ \text{: constant.} \end{cases}$$

The minimum cell size was 0.4 × 0.2 × 0.0625 mm^3 in the dielectric medium of $\varepsilon_r = 4.0$ in this model, thus, the CFL condition was $\Delta t \le 0.0416412$ ps. The time-step size was set as

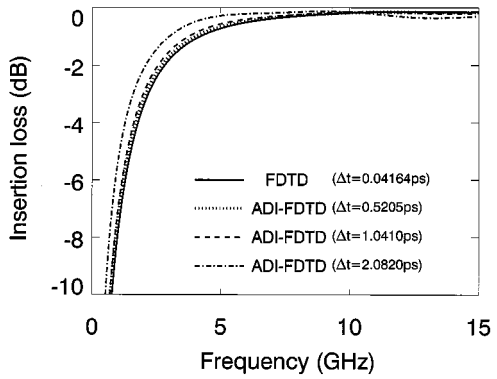

Fig. 8. Insertion loss versus frequency.

TABLE II
INFORMATION ON THE STRIPLINE SIMULATION

	Δt	Steps	CPU Time	Memory
FDTD	0.04164 ps	48030	216.0 s	2.0 Mb
ADI-FDTD	0.5205 ps	3840	95.2 s	3.9 Mb
ADI-FDTD	1.0410 ps	1920	48.3 s	3.9 Mb
ADI-FDTD	2.0820 ps	960	24.1 s	3.9 Mb

0.04164 ps for the conventional FDTD and 0.5205, 1.0410, and 2.0820 ps for the ADI–FDTD. The normalized output voltages at observation points versus time are shown in Fig. 7. The results in the ADI–FDTD case and conventional FDTD case are in good agreement. By applying the Fourier transformation of the excited pulse and output signal, the insertion loss was calculated. The results are shown in Fig. 8. As is clearly shown, an increase in the time-step size resulted in numerical error [8]. However, the results of the ADI–FDTD with $\Delta t = 0.5205$ ps, and $\Delta t = 1.0410$ ps almost agree with the results of the conventional FDTD. Table II provides information on this simulation. For the ADI–FDTD, if the time-step size is set 25 times as large as that of the conventional FDTD, total time steps can be reduced by a factor of 25. The CPU time is also reduced to 22%.

IV. CONCLUSION

This paper introduces the 3-D ADI–FDTD method for solving full vector Maxwell's equations. The algorithm of the method is unconditionally stable, thus, the limitation of the maximum time-step size does not depend on the CFL condition, but rather on numerical errors. What limits the maximum time-step size depends on what kinds of problems or models are calculated. If the size of the local minimum cell in the computational domain is much smaller than the wavelength, as in the examples shown in this paper, the error limitation is much larger than the CFL limitation and the 3-D ADI–FDTD method is more efficient than the conventional FDTD method.

REFERENCES

[1] K. S. Yee, "Numerical solution of initial boundary value problems involving Maxwell's equations in isotropic media," *IEEE Trans. Antennas Propagat.*, vol. AP-14, pp. 302–307, May 1966.
[2] A. Taflove, *Computational Electrodynamics*. Norwood, MA: Artech House, 1995.
[3] T. Namiki, "A new FDTD algorithm based on alternating direction implicit method," *IEEE Trans. Microwave Theory Tech.*, vol. 47, pp. 2003–2007, Oct. 1999.
[4] G. D. Smith, *Numerical Solution of Partial Differential Equations*. Oxford, U.K.: Oxford Univ. Press, 1965.
[5] T. Namiki, "The electromagnetic simulation system based on the FDTD method for practical use," presented at the Asia–Pacific Microwave Conf., Yokohama, Japan, Dec. 1998.
[6] W. H. Press *et al.*, *Numerical Recipes in FORTRAN*, 2nd ed. Cambridge, U.K.: Cambridge Univ. Press, 1992, pp. 42–43.
[7] G. Mur, "Absorbing boundary conditions for the finite-difference approximation of the time-domain electromagnetic field equations," *IEEE Trans. Electromag. Compat.*, vol. EMC-23, pp. 377–382, Nov. 1981.
[8] T. Namiki and K. Ito, "Investigation of numerical errors of the two dimensional ADI–FDTD method," *IEEE Trans. Microwave Theory Tech.*, to be published.

Takefumi Namiki (M'99) was born in Chiba, Japan, in 1963. He received the B.S. degree in physics from the Tohoku University, Sendai, Japan, in 1985, and is currently working toward the Ph.D. degree at the Chiba University, Chiba, Japan.

From 1986 to 1991, he was with Fujitsu Laboratories Ltd., Atsugi, Japan, where he was engaged in research of high-speed optical modulator for optical communications systems. In 1991, he joined Fujitsu Ltd., Tokyo, Japan, where he was engaged in research and development of the computational science, and since 1994, has been engaged in research of computational electromagnetics. His research interests include numerical techniques for modeling electromagnetic fields and waves, and computer-aided engineering (CAE) systems of microwave circuits, antennas, and optical waveguides.

Mr. Namiki is a member of the Institute of Electrical, Information and Communication Engineers (IEICE), Japan.